TWELFTH EUROPEAN ROTORCRAFT FORUM

Paper No. 43

HELICOPTER RESPONSE TO AN AIRPLANE'S VORTEX WAKE

Ki-Chung Kim
Graduate Student

and

Gunjit Bir
Research Associate

and

Inderjit Chopra
Professor

September 22-25, 1986

Garmisch-Partenkirchen
Federal Republic of Germany

Center for Rotorcraft Education and Research
Department of Aerospace Engineering
University of Maryland
College Park, MD 20742, USA

HELICOPTER RESPONSE TO AN AIRPLANE'S VORTEX WAKE

Ki-Chung Kim, Graduate Student
and
Gunjit Singh Bir, Research Associate
and
Inderjit Chopra, Professor

Center for Rotorcraft Education and Research,
Department of Aerospace Engineering
University of Maryland
College Park, MD 20742,USA

ABSTRACT

An analytical formulation is developed for studying the rotor-fuselage system response to an airplane's trailing vortex field. The blades are modeled as elastic beams undergoing flap bending, lag bending and torsional deflections. The fuselage is modelled as a rigid body with five degrees of freedom: longitudinal, lateral, vertical, roll and pitch. Quasisteady strip theory is used to obtain aerodynamic forces, and a dynamic inflow model is used to include the wake-induced unsteady effect. Dynamic stall and reverse flow effects are also included. The coupled rotor-fuselage equations are linearized about the vehicle trim state and the blade steady-state deflected position, and then solved by a numerical time-integration technique. Dynamic response results are determined in terms of blade deflections, blade stresses, rotor disk tilts, and hub loads and moments.

Results are calculated for four cases of vortex encounters: hovering helicopter with vortex axis aligned with hub center: hovering helicopter with descending vortex at 16 ft/sec.; helicopter flies along vortex axis; and helicopter flies across a two vortex system. For the vortex model, a fresh wake of a B-747 airplane is used and the response is calculated for typical helicopters including hingeless, articulated and teetering rotors.

NOTATION

a	= blade lift curve slope
c	= blade chord, m
C_d	= blade section drag coefficient
C_ℓ	= blade section lift coefficient
$C_{m_{ac}}$	= blade section moment coefficent about the aerodynamic center
$[C]$	= damping matrix in response equations
C_T	= thrust coefficient, $T/\pi\rho\Omega^2R^4$
C_{m_x}, C_{m_y}	= helicopter rolling and pitching moment coefficents
$[K]$	= stiffness matrix in response equations

$\underset{\sim}{\ell}$ $\underset{\sim}{m}$ = coefficient matrices in the dynamic inflow equations

L_u, L_v, L_w = blade aerodynamic forces per unit length in u,v,w directions

m_o = reference mass per unit blade length, N-sec^2/m^2
M^o = mass of the helicopter, N-sec^2/m
$[M]$ = mass matrix in response equations
M_ϕ = aerodynamic moment per unit length about elastic axis, N

N_b = number of blades

q = nodal displacment, m
R = rotor radius, m
$\underset{\sim}{r}_h$ = column vector of hub displacement, m

u,v,w = elastic displacments in x,y,z directions respectively, m
U_G, V_G, W_G = gust velocity components at a blade section, m/sec

U_R, U_T, U_P = air velocity components relative to a blade section in the negative ξ,η,ζ, directions respectively, m/sec
$\underset{\sim}{V}$ = column vector of gust velocity, m/sec

V_G = vortex velocity vector at a blade section, m/sec

x = r/R
x_B, y_B, z_B = blade coordinate in the inertial frame, m

x_h, y_h, z_h = displacements of the perturbed hub center w.r.t. the unperturbed hub-fixed frame, m
α = blade section angle of attack, rad
α_d = delayed angle of attack, rad

α_{ds} = dynamic stall angle, rad

α_{re} = flow reattachment angle, rad

α_{max} = maximum allowable delay angle, rad

α_s = perturbation shaft tilt, positive forward, rad

$\delta(\ )$ = virtual variation, also perturbation
λ = rotor inflow ratio
$\delta\lambda$ = perturbed inflow

μ = advance ratio, $V \cos\alpha_s/\Omega R$

ξ,η,ζ = deformed blade coordinates, m
σ = solidity ratio, $N_b c/\pi R$

ϕ = geometric twist, rad
ϕ_s = perturbation shaft tilt, positive advancing side down, rad
ψ = nondimensionalized time, Ωt
ψ_n = azimuth postion of blade n at time ψ
θ_{ds} = yawed flow angle, rad

θ_{FP} = climb angle in steady flight, rad

τ_L, τ_D, τ_M = time delay constants in the dynamic stall model, sec

Ω = rotor rotating speed, rad/sec

Subscripts and Superscripts

$(\dot{})$ = $\partial/\partial t$ ( )

o = steady-state value

INTRODUCTION

A helicopter flying in the wake of a large fixed-wing airplane may experience hazardous conditions. Steep velocity gradients induced by the wings trailing vortex system can cause large rolling and pitching moments, load factors and dynamic stresses on the rotor system. The ride quality and controllability of the helicopter can also be adversely affected. In order to establish a safe separation distance between the airplane and the following helicopter, it is necessary to assess the hazard to the helicopter exposed to the wing-vortex system. This paper formulates an analytical analysis to evaluate the dynamic response of a helicopter encountering the trailing wake of a transport airplane.

In the literature, only selected attempts have been made to study the wake-vortex response of a helicopter. In Ref. 1, a flight investigation was conducted for the first time to determine the response of a medium sized helicopter (UH-1H, gross weight 7200 lbs) to the the trailing vortex system of a fixed-wing airplane (C-54, gross weight 58000 lbs). This study showed no unsafe vortex penetrations. The maximum rotor blade structural loads monitored during the vortex penetration were quite nominal, and also, the helicopter altitude response was confined to small excursions in yaw angle. These results may have been due to a weak vortex strength of the given airplane. Recently, Curtis et al[2] used a simple analytical formulation to determine the rotor response caused by the trailing vortex of a large transport airplane. The blade is assumed to undergo a single degree flap motion and rotor response is calculated in a quasisteady sense from the balancing of only first harmonic motion. The gust field is taken as frozen and the helicopter is assumed to encounter the vortex-field by climbing steadily from below. Using this approach, the dominant features of uncontrolled response on a long time scale are captured. The study showed that the lateral/directional response amplitude was largest for hingeless and smallest for the teetering rotor. It was also concluded that the lightly damped short-period dutch roll mode of a helicopter may become uncontrollable in a strong vortex-wake.

In Refs. 3 and 4, an extensive finite element formulation was developed to study the response of a rotor-fuselage system due to a three-dimensional gust field. In the present paper, this analysis is extended to investigate the dynamic response of a rotor-fuselage system due to the vortex-wake of a fixed-wing airplane. The fuselage is modelled as a rigid body with five degrees of freedom: longitudinal, lateral, vertical, roll and pitch motions. The blades are modeled as elastic beams undergoing flap bending, lag bending and torsional deflections. Quasisteady strip theory is used to obtain aerodynamic forces, and a dynamic inflow model is used to include the wake-induced unsteady effect. A dynamic stall model proposed by Johnson[5] is used to introduce delay effects in

lift build-up and to include the effect of leading-edge vortices in the post stall state. Reverse flow effects are also included. A finite element analysis based on Hamilton's principle is used for structural modeling of the elastic blades. For calculations, the velocity distributions in a vortex wake shed by a typical transport airplane (B 747) are taken from Ref. 6. The analysis is developed for an arbitrary approach angle to the vortex field in both hover and forward flight.

The differential equations governing the vortex encounter problem are nonlinear with time-varying coefficients. There is no simple way to solve these equations directly. The problem is therefore solved in three phases: vehicle trim, blade azimuth-dependent steady response, and vortex-induced response. The vehicle propulsive trim solution is obtained from the nonlinear vehicle equilibrium equations and this gives the rotor control settings and the vehicle orientation for a prescribed flight condition (Ref. 7). The azimuth-dependent blade steady response is determined by solving iteratively the blade nonlinear periodic equations using the finite element in time procedure (Ref. 8). To reduce computation time, blade equations (finite element) are transformed to modal space using the rotating blade natural vibration characteristics. Coupled equations governing the rotor-fuselage response to vortex encounter are linearized about the vehicle trim and blade equilibrium positions. A fourth-order time integration scheme (Runge-Kutta) is used to solve the response equations for a specific vortex field. A force summation method is used to calculate the blade dynamic stresses.

Transient response due to a strong vortex system of a transport airplane (B747) is calculated for three different rotors: hingeless, articulated and teetering. Dynamic response results are determined in terms of blade deflections, blade stresses, rotor disk tilts, and hub loads and moments. The effects of several parameters on response are investigated, including penetration angle, vortex height and descent velocity, and forward speed.

FORMULATION

The formulation details are given in Refs. 3 and 4. The helicopter is modeled as a rigid fuselage with N_b elastic blades. The blades are modeled as elastic beams undergoing flap bending, lag bending and torsional deflections. The equation of motion for elastic blades are obtained for axial displacement u, lead-lag bending displacement v, flap bending displacement w, and elastic twist ϕ. These equations are given in Ref. 9.

The finite element formulation for the blade is based on Hamilton's principle

$$\int_{t_1}^{t_2} (\delta U - \delta T - \delta W)\, dt = 0 \qquad (1)$$

where δU, δT and δW are respectively the variation of strain energy, the variation of kinetic energy, and the virtual work done. The expressions for δU and δT are given in Ref. 9. The expression for δW is

$$\delta W = \int_0^R (Lu\delta u + Lv\delta v + Lw\delta w + M\phi\delta\psi)\, dr \qquad (2)$$

where L_u, L_v, L_w and M_ϕ represent the combined aerodynamic and hub motion induced inertia forces distributed along the blade length in the axial, lead-lag, flap and torsion directions respectively. These forces and moments are derived in Ref. 3.

The fuselage is assumed rigid and undergoes three translational (vertical, longitudinal and lateral) and two rotational (pitch and roll) degrees of motion. The fuselage equations of motion are expressed as hub equations and these consist of rotor aerodynamic forces, fuselage aerodynamic forces, gravity loads, vehicle and rotor inertia forces. These force and moment equations are defined in Ref. 3.

The aerodynamic forces are obtained using quasisteady strip theory and noncirculatory forces are also included. For a steady induced inflow model, a linear variation (Drees) is used. The effects of reversed flow are introduced in an approximate manner. For the wake-induced response, the unsteady aerodynamic effects are introduced in an approximate manner through a dynamic inflow modeling. A linear variation of the perturbed inflow is used:

$$\delta\lambda = \delta\lambda_0 + \delta\lambda_{1C} \times \cos\psi + \delta\lambda_{1S} \times \sin\psi \tag{3}$$

The inflow variables are related to the perturbation rotor aerodynamic forces and moments:

$$\underset{\sim}{m}\,\dot{\underset{\sim}{\delta\lambda}} + \underset{\sim}{\ell}\,\underset{\sim}{\delta\lambda} = \left\lfloor \delta C_T^A,\ -\delta C_{m_x}^A,\ \delta C_{m_y} \right\rfloor^T \tag{4}$$

where

$$\underset{\sim}{\delta\lambda} = \begin{Bmatrix} \delta\lambda_0 \\ \delta\lambda_{1C} \\ \delta\lambda_{1S} \end{Bmatrix} \tag{5}$$

The δC_T, δC_{m_x} and δC_{m_y} are the perturbation thrust, roll moment and pitch moment respectively. The matrices $\underset{\sim}{m}$ and $\underset{\sim}{\ell}$ are adapted from Ref. 11. The elements of matrix $\underset{\sim}{\ell}$ are modified to account for the change in the air mass flow through the rotor disk caused by the vortex field and hub motion.

To include the effects of high angle of attack flows caused by vortex field, a dynamic stall model is used. Dynamic stall is characterized by a delay in flow separation due to the unsteady angle of attack, and by a vortex shedding from the leading edge of the airfoil when stalls initiates. In the present paper, a dynamic stall model proposed by Johnson[5] is used. The corrected aerodynamic coefficients are

$$C_\ell(d) = \sec^2\theta_{ds}\left[\frac{\alpha}{\alpha_d}\left\{C_\ell(\alpha_d \cos^2\theta_{ds}) - C_\ell(0)\right\} + C_\ell(o)\right]$$

$$+ \Delta C_\ell$$

$$C_d(\alpha) = \sec\theta ds\ Cd\ (\alpha d \cos\theta ds) + \Delta Cd \tag{6}$$

$$C_m(\alpha) = C_m\ (\alpha_d \cos^2 \theta_{ds}) + \Delta C_m$$

where

$$\theta_{ds} = \cos^{-1} \sqrt{\frac{U_T^2 + U_P^2}{U_T^2 + U_P^2 + U_R^2}} \tag{7}$$

The angle θ_{ds} is the yawed flow angle, α_d is the delayed angle of attack, and ΔC_ℓ, ΔC_d, ΔC_m are the increments in the aerodynamic coefficients caused by the leading-edge vortex. The angle α_d is a function of the time derivative of the angle of attack.

$$\alpha_d = \alpha - \min\left(\tau \left|\frac{\dot{\alpha}_C}{U_T}\right|, \alpha_{max}\right) \text{sign}(\dot{\alpha}) \tag{8}$$

where τ is the normalized time constant and its value depends on whether C_ℓ, C_d, or C_m is to be calculated. The increments ΔC_ℓ, ΔC_d, and ΔC_m occur when the section angle of attack reaches the dynamic stall angle α_{ds} (about 3° above the static stall angle) and a leading-edge vortex is shed. It is assumed that these increments build up linearly to their maximum values in an azimuth interval of 15° and then fall linearly to zero in the same azimuth interval. The peak values of ΔC_ℓ, ΔC_d, and ΔC_m are functions of the pitch rate α; the expressions are given in Ref. 5. After the transient loads die out, dynamic stall does not occur unless the flow is reattached; flow reattachment occured when α falls below α_{re} (just below the static stall angle).

VORTEX MODEL

A vortex model for the fresh wake of Boeing 747 is used[6].

$$V(r) = V_c\ [1 + \ell n \frac{r}{r_c}] \qquad r > r_c \tag{9}$$

$$V(r) = V_c \frac{r}{r_c} \qquad r \leq r_c \tag{10}$$

where V_c and r_c are vortex core tip speed and radius respectively. For the present results, the values for V_c and r_c are respectively taken as 16 m/sec and 2.51 m. The gust components, U_G, V_G and W_G of the vortex fields are functions of space and time. Therefore, the expressions for U_G, V_G and W_G are obtained for various radial and azimuthal locations.

The vortex-wake field is expressed as a velocity vector at the blade section, and which in turn can be expressed in terms of three velocity components along the unperturbed hub fixed coordinates.

$$\overline{V}_G(x,\psi_n,\psi) = U_G(x_B,y_B,z_B,t)\,\vec{i}_x + V_G(x_B,y_B,z_B,t)\vec{i}_y + W_G(x_B,y_B,z_B,t)\vec{i}_z \tag{11}$$

where x_B, y_B and z_B are blade coordinates in the inertial frame and these can be rewritten as

$$\begin{aligned} x_B &= -\mu\psi \cos\theta_{FP} + x_h + x\cos\psi_n \\ y_B &= y_h + x\sin\psi_n \\ z_B &= \mu\psi \sin\theta_{FP} + z_h \end{aligned} \tag{12}$$

The x_h, y_h and z_h are displacements of perturbed hub center with respect to the unperturbed hub-fixed frame. The ψ is a nondimensional time (Ωt) and ψ_n represents the azimuth position of blade n at time ψ.

The components of gust velocity vector (U_G, V_G, W_G) depend on the orientation of the vortex and the perturbed position of rotor. For example, for a hovering helicopter exposed to a descending vortex (Fig. 1(b)), these velocity components can be defined as

$$\begin{aligned} U_G(x_B,y_B,z_B,t) &= 0 \\ V_G(x_B,y_B,z_B,t) &= V(r)\,\frac{z_B - z_1}{[y_B^2 + (z_B-z_1)^2]^{1/2}} \\ W_G(x_B,y_B,z_B,t) &= -V(r)\,\frac{y_B}{[y_B^2 + (z_B-z_1)^2]^{1/2}} - V_d \end{aligned} \tag{13}$$

$$z_1 = z_I - V_d\,\psi$$

where z_I denotes the position of the vortex center with respect to the rotor hub at time $\psi = 0$.

SOLUTION PROCEDURE

Equations representing the rotor-fuselage dynamics are nonlinear and involve time dependent coefficients. There is no simple way to solve these equations directly. The problem is therefore divided into three phases: vehicle trim, blade steady response and vortex-induced response. The propulsive trim solution is obtained by solving iteratively the nonlinear vehicle equilibrium equations for the steady flight condition. Rigid blade modeling is used for this purpose. The trim solution gives the rotor control inputs (θ_o, θ_{1S}, θ_{1C}), the

vehicle orientation (α_s, ϕ_s) and the inflow λ. The second phase involves the

determination of the azimuth-dependent blade equilibrium position in a steady flight condition. To reduce computation time, the blade equilibrium equations in terms of nodal displacements (finite element) are transformed to modal space using the rotating blade coupled natural vibration characteristics. The resulting normal mode equations are solved using finite element in time procedure (see Ref. 8 for details).

The final phase involves the determination of the transient response of the rotor-fuselage system due to vortex fields generated by a fixed-wing airplane. The response equations are linearized about the steady-state vehicle trim and the azimuth-dependent blade equilibrium position. The linearized blade equations, fuselage equations and the dynamic inflow equations can be put in the matrix form

$$[\overline{M}(\hat{q}_o,\psi)] \begin{Bmatrix} \ddot{\hat{q}} \\ \underset{\sim}{\ddot{\delta\lambda}} \\ \ddot{\Gamma}_h \end{Bmatrix} + [\overline{C}(\hat{q}_o,\psi)] \begin{Bmatrix} \dot{\hat{q}} \\ \underset{\sim}{\dot{\delta\lambda}} \\ \dot{\Gamma}_h \end{Bmatrix}$$

$$+ [\overline{K}(\hat{q}_o, \dot{\hat{q}}_o, \underset{\sim}{\lambda}, \underset{\sim}{V}, \Gamma_{ho}, \psi)] \begin{Bmatrix} q \\ \underset{\sim}{\delta\lambda} \\ \Gamma_h \end{Bmatrix} = \{\overline{Q}(\hat{q}_o, \Gamma_{ho}, \underset{\sim}{V}, \psi)\} \qquad (14)$$

where

$$\{\hat{q}\} = [\underline{q}^1 \ \underline{q}^2 \ \ldots \ \underline{q}^{N_b}]^T \qquad (15)$$

Equations (13) are transformed to the modal space using the first few natural modes (2 flap, 2 lag, 2 torsion) for the blade. The coupled normal mode response equations can be written as

$$[M^*] \{P\} + [C^*] \{P\} + [K^* (\underset{\sim}{\lambda}, \underset{\sim}{V})] \{P\} = \{Q^*(\underset{\sim}{V})\} \qquad (16)$$

where

$$\{P\} = [\xi_1^{(1)}, \xi_2^{(1)}, \ldots \xi_6^{(1)} \xi_1^{(2)} \ldots \xi_6^{(N_b)} \lambda_o, \lambda_{1C}, \lambda_{1S}, \Gamma_h, \alpha_s, \phi_s] \qquad (17)$$

The final equations (16), representing the coupled rotor-fuselage response due to fixed-wing airplane's trailing vortex, are solved using a time integration technique.

Results and Discussion

Numerical results are obtained for three different rotor configurations: hingeless, articulated and teetering. The blade and fuselage structural

properties of these rotors are listed in Table 1. It has been observed that vortex-induced responses of these rotors show similar trends. Therefore, for brevity, a detailed examination of dynamic response for the hingeless rotor which appears to be more susceptible to the vortex encounter is made. Also, for comparison some of the responses of articulated and teetering rotors are presented.

Results are obtaind for a four-bladed hingeless rotor (soft-inplane) with Lock number $\gamma = 5$, thrust level $C_T/\sigma = 0.1$, solidity ratio $\sigma = 0.05$ and zero precone. The blade static airfoil characteristics used are

$$C_\ell = 6.28\alpha, \quad \alpha \leq 12°$$

$$= 1.315, \quad \alpha > 12°$$

$$C_d = 0.0095$$

$$C_{m_{ac}} = 0$$

These characteristics are modified by dynamic stall effects. The delayed lift, drag, and moment coefficients are calculated using time lag factor $\tau_L = 4.8$, $\tau_D = 2.7$ and $\tau_M = 2.7$. The dynamic stall angle is assumed to be $15°$ (3° above the static stall angle). The peak values of the vortex-induced increments in lift, drag, and moment coefficients are: $\Delta C_\ell = 2.0$, $\Delta C_d = 0$, and $\Delta C_m = -0.65$. The flow reattachment is assumed to take place at the static stall angle.

Numerical results are calculated for uncontrolled response (fixed pilot controls) of the rotor-fuselage system due to the vortex wake. Results are presented for four cases of helicopter encounter with the wing-vortex system, shown in Figs. 1(a)-1(d). For comparison, steady response results in terms of blade tip deflection and bending moments at blade root are presented in Table 2. It is observed that these steady responses show primarily second harmonic components.

Case I: Hover---Hub center aligned along vortex axis (Fig. 1(a))

A hovering helicopter encounters the vortex at time $\psi = 0$ with the hub longitudinal axis aligned with the vortex axis (Fig. 1(a)). The vortex induces an antisymmetric velocity field over the rotor disk (downflow at the advancing side, upflow at the retreating side). Figs. 2-6 describe the helicopter perturbation response subsequent to vortex encounter. In all figures, the zero value on the vertical axis represent the trimmed response condition.

Fig. 2 shows tip deflections due to flap bending, lag bending and torsion modes for blade 1. Blade 1 refers to the blade located at the rearward position at time $\psi = 0$. The vortex-induced oscillatory flap response attains the maximum value ($\sim 4.5°$) in about 3 cycles. The flap response shows a 1/rev variation. This is because the vortex field is antisymmetrically distributed on the disk and hence induces periodic aerodynamic forces. The lag response shows a 0.7/rev component initially, which is the rotating lag natural frequency and then it becomes 1/rev variation. The lag response is quite comparable to flap response, and again it attains the maximum amplitude ($\sim 1.5°$) in about 3 cycles. The pitch response is negligible compared to the flap and lag motions and shows a 5/rev variation, which is the rotating torsional natural frequency. Also there appears to be a weak coupling of lag motion with torsion motion.

Fig. 3 presents the rotor flap response (combined from all blades) in the fixed reference frame after the rotor encounters the vortex-wake. The rotor response is shown in terms of coning angle, and the longitudinal and lateral tilts of tip-path plane. Because of the antisymmetric nature of wake-induced loads the coning angle is not disturbed. The longitudinal tip-path plane tilt (equivalent to β_{1C}) is defined positive for nose-down tilt, and the lateral tip-path plane tilt (equivalent to β_{1S}) is positive for advancing side up. Both these tilts are defined with respect to the shaft axis. The rotor response builds to the peak forward tilt of 4.5° in about 3 cycles, at the time when maximum flap response occurs. Immediately after the wake hits the rotor, there is a negative disk tilt (advancing-side down) and then in about 3 cycles it settles down to a comparatively small positive sideward tilt. As expected, an oscillatory aerodynamic forcing due to vortex wake would induce a flap response with a phase lag of about 90° resulting in a predominant forward tilt for the present case. The vibratory components of disk tilts are small and occur at 4/rev.

Fig. 4 shows flap bending and lag bending moments at the root of blade 1 (non-dimensionalized with respect to $m_o\Omega^2R^3$). These effectively represent the blade flexural stresses at the root and are calculated using a force summation method. Flap moment is calculated about the η-axis at the blade root and is positive if the upper surface is in compression. Lag moment is calculated about the ζ-axis at the blade root and is positive if the leading-edge is in compression. The flap bending moment contains primarily a 1/rev component and a small 2/rev component. A 1/rev component flap moment appears quite in phase with the flap response (Fig. 2). The lag moment is quite comparable with the flap moment and is dominated by the component. Again these moments achieve the steady state value in about 3 cycles.

Fig. 5 presents the time history of hub rolling and pitching moments transferred to the airframe. These moments cause vehicle vibration, and also are important for establishing control margins. The positive pitching moment is nose-up and the positive rolling moment is advancing-side-down. One observes the 4/rev variation of moments with this 4-bladed rotor. The oscillatory components of pitching moment is larger than that of rolling moment. Also the vehicle experiences a considerable negative steady pitching moment (nose down) occuring within a short period time (2 cycles) after the vortex encounter. This perhaps indicates the necessity for very rapid pilot control inputs to maintain trim.

Fig. 6 shows the load factor experienced by the soft-inplane rotor. The load factor is the ratio of the vertical force experienced by the hub to the gross weight of the vehicle. Because the velocity components of the vortex averages out around the rotor disk (anti-symmetric), there is a neglible variation in load factor. Thus, the impact of the vortex encounter is primarily absorbed by the rotor, affecting only hub moments of the vehicle for this case.

Comparing the vortex-induced response results in hover with the steady response (trimmed) value for a high forward speed of μ = .4 (Table 2), one observes that the perturbed amplitudes are quite large. For example, perturbed flap and lag amplitudes are about same values as high speed steady values, whereas the flap and lag moments are about three times the steady values. This means that a sudden encounter with a vortex can overstress the blade.

Case II: Hover ---Descending vortex (Fig.1 (b))

This case considers a hovering helicopter exposed to a descending vortex. At time $\psi = 0$, the rotor hub center is located at one radius below the vortex axis, then the vortex descends vertically at a speed of 16 ft/sec (Fig.1 (b)). Results for this case are presented in Figs. 7-11.

Fig. 7 shows tip response amplitudes due to flap bending, lag bending and torsional modes. The flap response builds up during the first 7 cycles and then slowly decays. The maximum flap response amplitude is about 4.5° and it occurs when the vortex axis passes the rotor disk plane. The lag response shows 0.7/rev component for the first few cycles and then gradually changes to a 1/rev variation. The maximum amplitude of lag response is about 1°. Again, the maximum lag amplitude occurs when the vortex axis passes through rotor hub. Comparing with Case I where the rotor is held in the vortex wake, the peak flap response is nearly the same as observed earlier but the peak lag response is reduced by 20%.

Fig. 8 represents the disk tilt variation with time. Due to the descending speed of the vortex, there is a small negative coning angle. The maximum longitudinal tilt ($\sim$ 4°) occurs at 7 cycles, the time when the vortex axis lies on the rotor disk. The maximum lateral tilt is 1.3 degree and it occurs at about 4.5 cycles. Comparing with Case I, the maximum amplitude of longitudinal disk tilt is nearly the same, whereas the lateral disk tilt is somewhat different. A larger lateral disk tilt around 4 cycles is induced by the negative coning angle.

Fig. 9 shows flap bending and lag bending moments at the blade root. Again, the maximum values of these moments occur around the 7th cycle of time when the vortex axis lies on the rotor disk. The peak amplitudes of vibratory bending moments are respectively reduced by 7% in flap bending and 22% in lag bending as compared to Case I. This reduced impact on blade stress may be due to a gradual penetration into the vortex field.

Fig. 10 presents the time history of hub pitching and rolling moments. The oscillatory pitching moment rapidly builds up for the first 7 cycles and then rapidly dies out. Comparing with Case I, it is observed that the peak magnitudes of both pitching and rolling moments are only slightly affected by the descent speed.

Fig. 11 shows the load factor experienced by a helicopter exposed to a descending vortex. Compared to Case I, the load factor is influenced by the descending velocity of the vortex. Immediately after the helicopter is exposed to the vortex wake, there is a downward push (unloading of hub by 1/4 g) and then it gradually recovers to the steady-state value of one.

It is shown that Case II of the descending vortex is less critical to the helicopter than Case I of a stationary vortex aligned with rotor hub. The lag response, bending stresses, as well as hub loads are somewhat reduced for Case II. It is interesting to note that the maximum oscillatory flap response is not affected with the descent speed of the vortex as long as its axis is aligned with the hub. However, with descending vortex, one needs to carry out many extra cycles of time integration to capture the peak values.

Case III: Forward flight --- Helicopter flies along vortex axis (Fig.1 (c))

Case III considers a helicopter flying along the vortex centerline at an advance ratio of 0.3. At time $\psi = 0$, the rotor is exposed to the vortex field

with its longitudinal axis aligned with vortex axis (Fig.1 (c)). Results are presented in Figs. 12-15 for this case.

Fig. 12 shows the perturbation flap, lag and pitch response amplitudes induced by the vortex-wake. These blade responses show trends similar to those observed for Case I for a hovering helicopter (Fig.2). The maximum tip amplitudes for flap and lag bending are about 4.5° and 1.5°, respectively. Thus, the vortex-induced blade responses are only slightly affected by forward speed. Fig.13 shows the coning angle and disk tilts variation with time for this case. The general trends are quite similar to those observed for a hovering helicopter (Fig.3). The maximum longitudinal tilt is 3.6° and it occurs at about 3 cycles of time after rotor is exposed to the wake. The amplitude of vibratory components (4/rev) in lateral tilt is larger (by a factor of two) than that of hovering helicopters. Also there is a small variation in coning angle due to forward speed. In Fig. 14, the vortex-induced flap and lag bending variations are similar to those for Case I of hovering rotor (Fig.4). The maximum amplitude of root bending moments are only slightly affected by forward speed.

Fig. 15 shows the hub rolling and pitching moment induced by the vortex-wake. Comparing with result for Case I of the hovering rotor (Fig.5), the vortex-induced hub moments are quite different in forward flight. The oscillatory amplitude of pitching moment is reduced by more than 50% whereas that of the rolling moment is increased by about 50%. This difference stems from the assymetric flow environment on the rotor disk due to forward flight.

The load factor experienced by the hingeless rotor for this case is presented in Fig. 16. The helicopter initially experiences a downward acceleration but it recovers quickly. However, there is a sizable fluctuation in the load factor for this case as compared to Case I of the hovering rotor (Fig.6). At the hub, the vehicle experiences about .2g peak-to-peak vibration at 4/rev frequency.

From the comparison of results between hover and forward flight for an identical vortex exposure, one observes that the rotor perturbation responses, such as blade tip response and blade bending moments, depend on the vortex field which the helicopter is exposed to, but the vehicle responses such as hub moments variation, and load factor variation depend on the vortex field as well as the forward speed.

Case IV: Forward flight ---Helicopter flies across two vortex system (Fig. 1(d))

Case IV considers a helicopter flying across two vortices (Fig.1 (d)). Looking from aft of the fixed wing, the helicopter approaches the pair of vortices from the left and flies across the two vortices at a low forward speed, $\mu = 0.15$. At time $\psi = 0$, the helicopter is five-radius distance away from the left vortex center and is exposed to vortex field. At this point, since the vortex-induced disturbances are quite weak, it is possible for the pilot to bring the vehicle to a trimmed state. Uncontrolled response results are presented in Figs. 17-21 for the case.

Fig. 17 shows the tip deflections due to flap bending, lag bending and torsional motions. As the helicopter approaches from the left side, the oscillatory flap response builds up because of the wake upwash, then reduces and becomes negative due to downwash between the two vortices. The flap response becomes positive again as the helicopter flies across the right vortex axis. The maximum flap response is negative 3.5° (downward) when the helicopter is

near the left vortex axis and is positive 3.5°(upward) as the helicopter passes by the right vortex axis. The flap response shows 1/rev variation. The peak to peak lag response amplitude is as the large as flap response for most of the time. The pitch response is quite negligible all the time. Comparing with Case III of one helicopter flying along the vortex axis (Fig.12), the peak flap response is very much reduced (more than 50%), whereas the peak lag response increases (by one third) for this case.

Fig. 18 presents the variations of the rotor coning angle and disk tilts as the helicopter flies across the vortices. The coning angle variation follows closely the velocity field distribution induced by the two vortices (Fig. 1 (d)). The maximum longitudinal tilt is about 1° and it occurs when the helicopter passes by each vortex axis. The maximum lateral tilt is about 2° and again, it occurs when the helicopter crosses each vortex axis.

Fig. 19 shows root bending moments for blade 1. Both flap and lag bending moments are in phase with the flap and lag motions respectively. Comparing with the result for Case III (Fig. 13), the flap bending moment is much reduced (by 50%), whereas the lag bending moment is increased (by 30%) for this case.

Fig. 20 presents the hub rolling and pitching moment variations. It is shown that whenever the helicopter crosses the vortices, there are considerable variations in both pitching and rolling moments. These hub moments show 4/rev oscillations. The nature appears somewhat similar to the variations of longitudinal and lateral disk tilts of these moments.

Fig. 21 shows the load factor experienced by the fuselage for this case. Both the maximum upload and maximum download values are about .7g from the steady state condition. Comparing with the result of Case III (Fig.16) where the helicopter flies along the vortex axis and experiences small periodic 4/rev fluctuations, in the present case when helicopter flies across vortices it experiences large period oscillations due to upwash, downwash and followed by again upwash velocity distributions. These large period oscillations in load factor may not be as uncomfortable as the previous short period oscillations observed for Case III.

The earlier results were obtained for a typical hingeless rotor. In Figs. 22-25, the perturbed response results for a typical articulated rotor are presented. For calculations, a four-bladed rotor with flap and lag hinge offsets of 6% from these rotation axis is used. The aerodynamic characteristics of this rotor are chosen to be same as those of the hingeless rotor defined earlier. The general behavior of the responses of articulated rotor is similar to that of hingeless rotor. Results are presented only for Case IV where the helicopter flies across two vortices (Fig.1 (d)). Fig. 22 shows vortex-induced tip response amplitudes. The nature of the response motions is quite similar to the one observed earlier for a hingeless rotor (Fig.17), with the obvious exception that lag motion vibration frequency is now reduced to .3/rev. Fig. 23 presents the vortex-induced coning angle and disk tilts as the helicopter flies across the vortices. Again, these results are quite similar to those observed for a hingeless rotor (Fig. 18), except that a larger lateral disk tilt for an articulated is observed. Fig. 24 shows the variations of the hub rolling and pitching moments for the articulated rotor. As compared to the hingeless rotor (Fig. 20), the trend of these moment variations are quite similar as expected, but the amplitudes of these moments are sizably reduced. Further, it is interesting to note that the load factor variation with time (Fig. 25) is not much affected with an articulated rotor.

Figs. 26-29 present the results of a teetering rotor for an identical exposure to a vortex-wake (Case IV). It is a two-bladed rotor with flap hinge at the rotation axis (flap frequency = 1/rev) and stiff lag blade (lag frequency = 1.4/rev). Fig. 26 shows vortex-induced tip deflections. The general trend is similar to those for hingeless and articulated rotors. The amplitude of lag response is small for a teetering rotor, possibly due to larger lag stiffness (stiff-inplane). Fig. 27 presents the flap and lag bending moment variations. Compared to the results for hingeless rotors (Fig. 19), the amplitudes of these moments are very much reduced. Fig. 28 shows the time history of hub moments variations. The trends are quite similar to those of hingeless and articulated rotors. Also, the load factor experienced by the teetering rotor (Fig. 29) is quite similar to those observed for hingeless and articulated rotors.

Conclusions

The dynamic response of the rotor-fuselage system to an airplanes trailing vortex has been investigated using a finite element formulation. The analysis was formulated for both hover and forward flight for three different rotor configurations: hingeless, articulated and teetering. The response has been calculated in terms of blade deflections (flap, lag and torsion), blade bending moments, rotor disk tilts, load factors, and hub loads and moments. Numerical results are calculated for four cases of vortex encounters, of which two are hover (Case I and II) and two are forward flight (Case III and IV). The following conclusions are drawn from this study.

1. A hovering helicopter exposed to a stationary vortex field (Case I) experiences flap response (at tip) about 4.5°, lag response (at tip) about 1.5°, and negligible torsional response.

2. The vortex-induced flap and lag bending moments at the blade root for a hingeless rotor in hover (Case I) are about three times the steady values experienced in a high forward speed (μ = .4).

3. For hovering flight (Case I), the vortex-wake induces a comparatively large-longitudinal disk tilt (about 4.5°) and a larger pitching moment than rolling moment. The load factor is not affected.

4. A gradual descent of the vortex-wake on a hovering helicopter (Case II) is less critical than the stationary vortex exposure. The peak values of lag response, bending stresses and hub loads are reduced, whereas the flap response is not affected with vortex descent speed.

5. A helicopter flying along the vortex axis (Case III) experiences blade bending responses and stresses quite identical to those experienced in hovering flight, whereas vortex-induced hub moments and load factors, depend on the forward speed also.

6. A helicopter flying across a two vortex system (Case IV) experiences a different type of response than one flying along the vortex axis. The peak values of blade flap response and flap bending (at the root) are reduced by one-half, and lag response and lag bending are increased by one-third. Also, there are considerable fluctuations in the load factors and hub moments.

7. A helicopter flying along the vortex axis experiences a .1g (half peak-to-peak) high frequency (4/rev) load factor variation, whereas by flying across the two vortices it experiences .7g large period oscillations in load factor.

8. The general response of different rotors to the vortex-wake show similar trends. The response of the hingeless rotor shows large amplitudes as compared to articulated and teetering rotors.

Acknowlegement

This research work is supported by DOT/Transportation Systems Center under Contract no. DTRS-57-85 C00105. The authors acknowledge helpful discussions with Dr. David Burnham who is also technical monitor of this grant.

References

1. W.R. Mantay, G.T. Holbrook, R.L. Campbell, R.L. Tamaine — Helicopter Response of an Airplane's Trailing Vortex Journal of Aircraft (1977) 4 (14) 357-363.

2. H.C. Jr. Curtiss, Z. Zhou — The Dynamic Response of Helicopters to Fixed Wing Aircraft Wake Encounters Vertical Flight Technology Seminar (1985) held at Peking, China.

3. G.S. Bir, I. Chopra — Gust Response of Hingeless Rotors J. of American Helicopter Society (1986) 4 (31) 33-46

4. G.S. Bir, I. Chopra — Prediction of Blade Stresses due to Gust Loading 11th European Rotorcraft Forum (1985) 9 (73).

5. W. Johnson — A Comprehensive Analytical Model of Rotorcraft Aerodynamics and Dynamics: Part I NASA TM-81182 (1980) 6.

6. D.C. Burnham — B-747 Vortex Alleviation Flight Tests: Ground Based Sensor Measurements DOT-FAA-RD-81-99 (1982) 2.

7. B. Panda, I. Chopra — Flap-Lag-Torsion Stability in Forward Flight J. of American Helicopter Society (1985) 10 (30) 30-39.

8. B. Panda, I. Chopra — Dynamic Stability of Hingeless and Bearingless Rotors in Forward Flight Vertica, 10th Anniversary Issue 1986.

9. N.T. Sivaneri, I. Chopra — Finite Elment Analysis for Bearingless Rotor Blade Aeroelasticity J. of American Helicopter Society (1984) 4 (26) 42-51.

10. C.H. Hong, I. Chopra — Aeroelastic Stability Analysis of a Composite Rotor Blade
J. of American Helicopter Society (1985) 4 (26) 57-67.

11. D.M. Pitt, D.A. Peters — Theoretical Prediction of Dynamic Inflow Derivatives
Vertica (1981) 5 (1).

Table 1 Blade and Fuselage Strucutural Properties

Flapwise $EI_y/m_o\Omega^2R^4$	= 0.014486
Chordwise $EI_z/m_o\Omega^2R^4$	= 0.026655
	= 0.166500 (teetering)
Torsion $GJ/m_o\Omega^2R^4$	= 0.005661
Flapwise inertia k^2m_1/R^2	= 0
Chordwise inertia k^2m_2/R^2	= 0.000625
Polar area moment k_A^2/R^2	= 0.001398
Helicopter rolling moment of inertia I_{xH}/MR^2	= 0.037
Helicopter pitching moment of inertia I_{yM}/MR^2	= 0.097

Table 2 Steady Response Results

Half peak-to-peak amplitude		Advance ratio μ = .15	μ = .3	μ = .4
Tip deflections	ν	0.0123	0.0154	0.0231
	ω	0.0146	0.0307	0.0732
	φ	0.0003	0.0011	0.0015
Flap bending moment	M_η	0.0013	0.0021	0.0043
Lag bending moment	M_ζ	0.0018	0.0026	0.0032

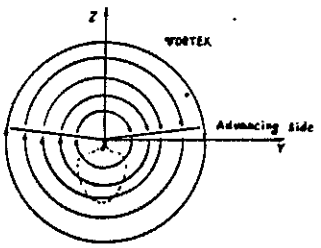

Fig.1 (a) Hovering (Looking from behind) CASE I

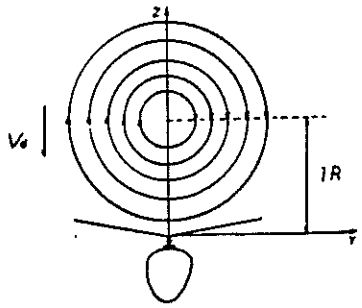

Fig.1 (b) Hovering – Descending Vortex CASE II

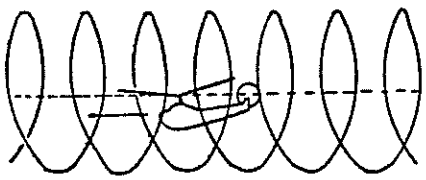

Fig.1 (c) Helicopter flying along the vortex axis CASE III

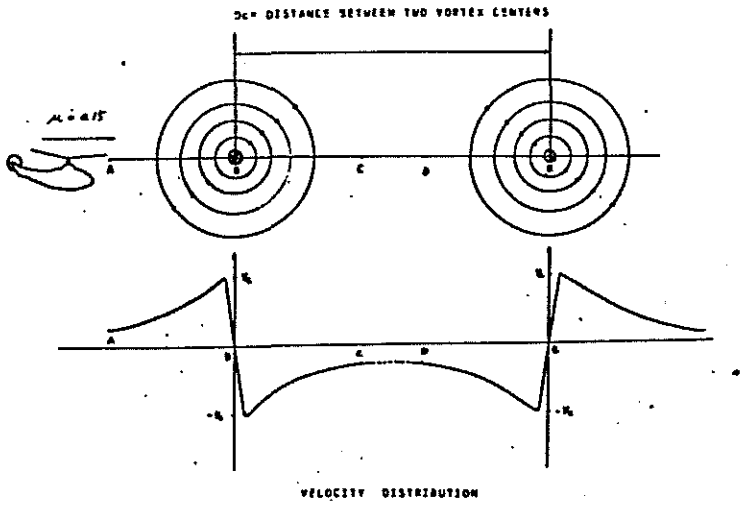

Fig. 1 (d) Helicopter flying across the two vortices CASE IV

Fig.2 Flap, lag torsion bending deflections

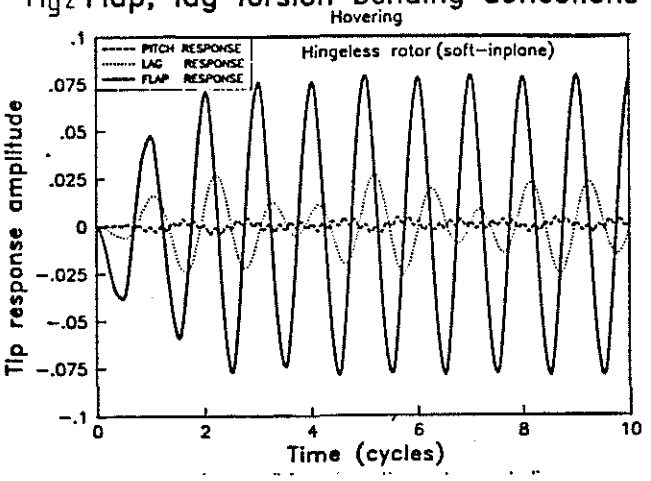

Fig.3 Disk tilt variation with time

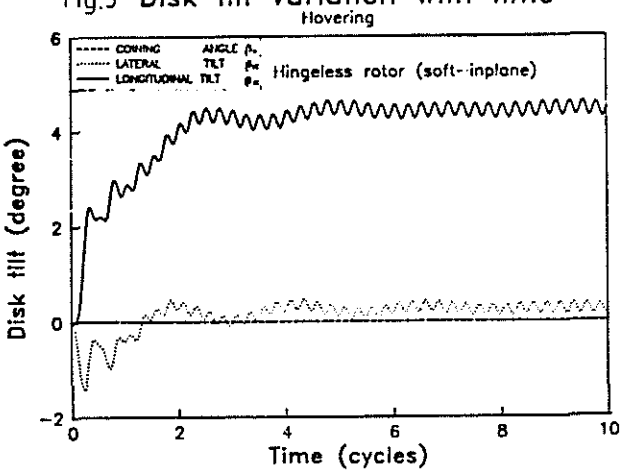

Fig.4 Bending moments of soft-inplane rotor

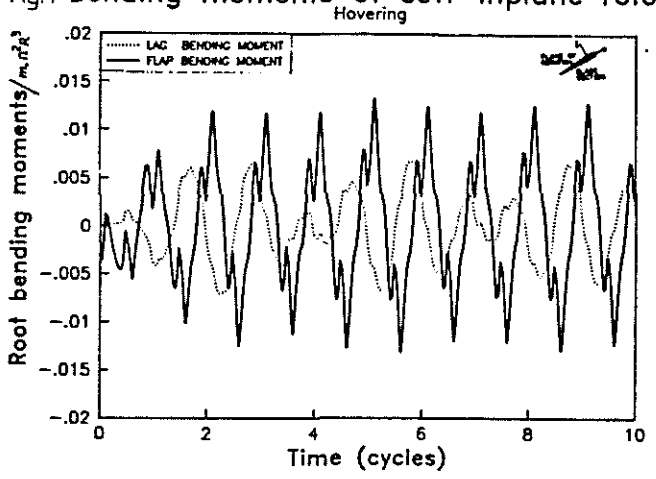

Fig.5 Hub moments of soft-inplane rotor

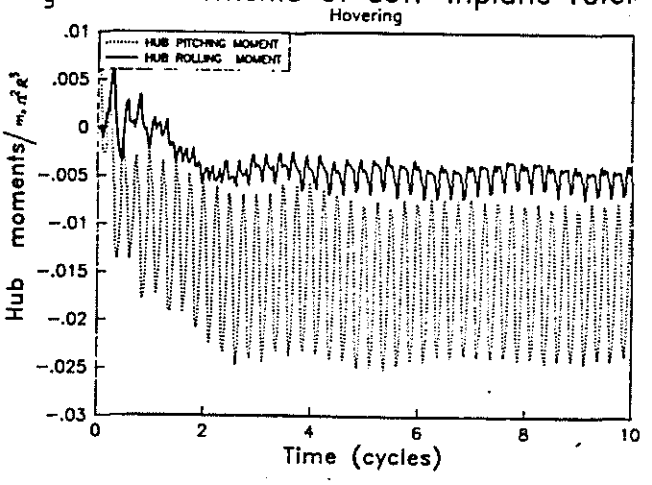

Fig.6 Dynamic response of soft-inplane rotor

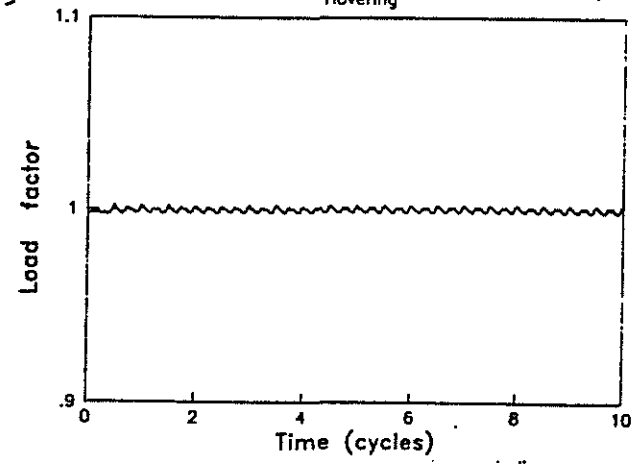

Fig.7 Flap, lag and torsion bending deflections

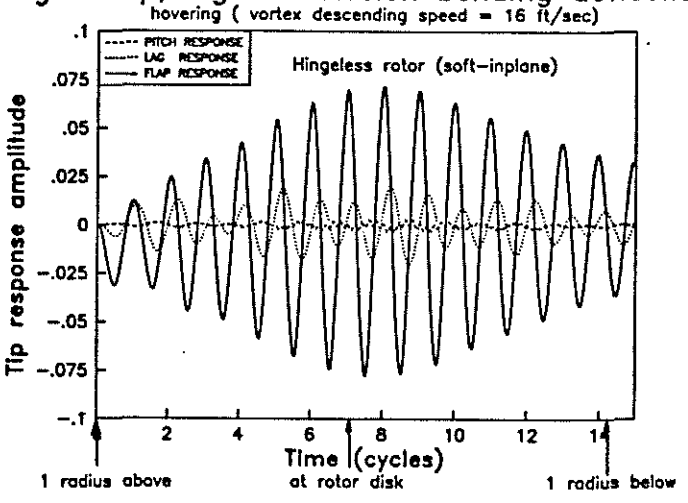

Fig.8 Disk tilt variation with time

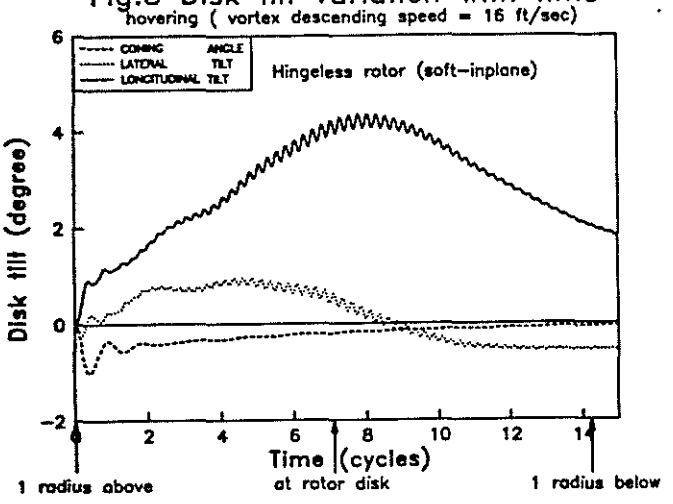

Fig.9 Bending moments of soft-inplane rotor

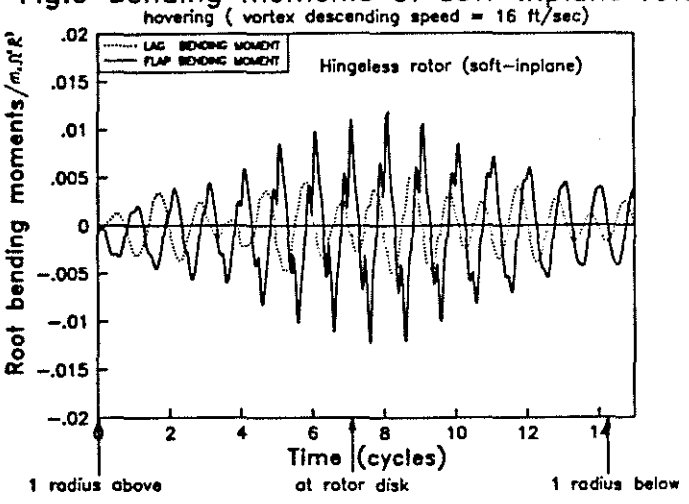

Fig.10 Hub moments of soft-inplane rotor

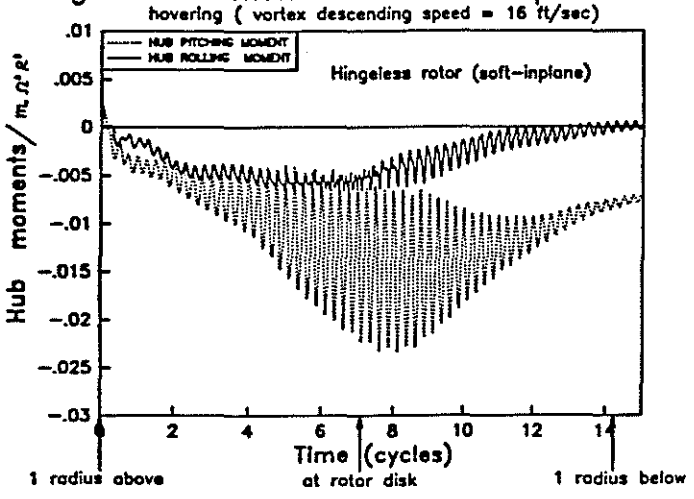

Fig.11 Dynamic response of soft-inplane rotor

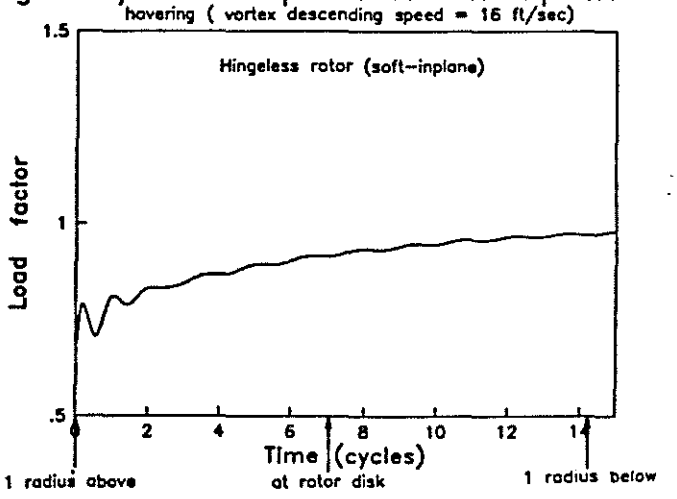

Fig.12 Flap, lag torsion bending deflections

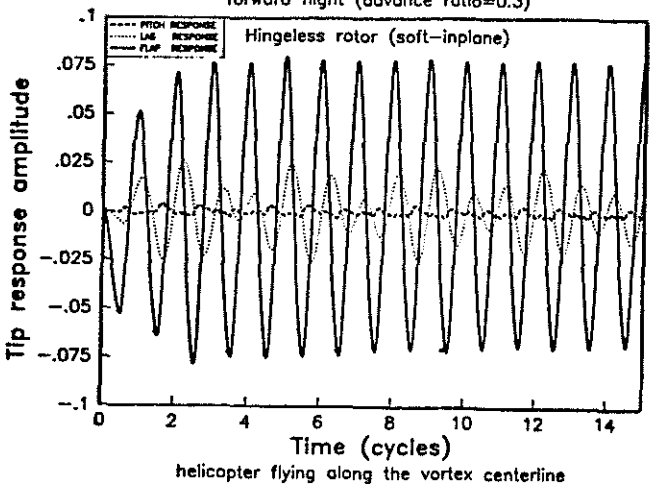

Fig.13 Disk tilt variation with time

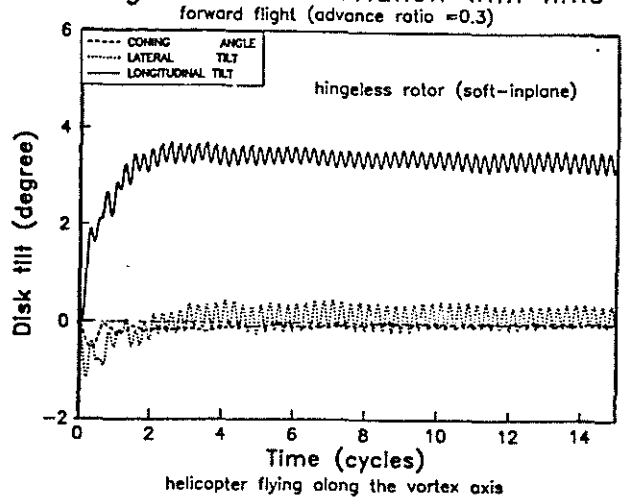

Fig.14 Bending moments of soft-inplane rotor

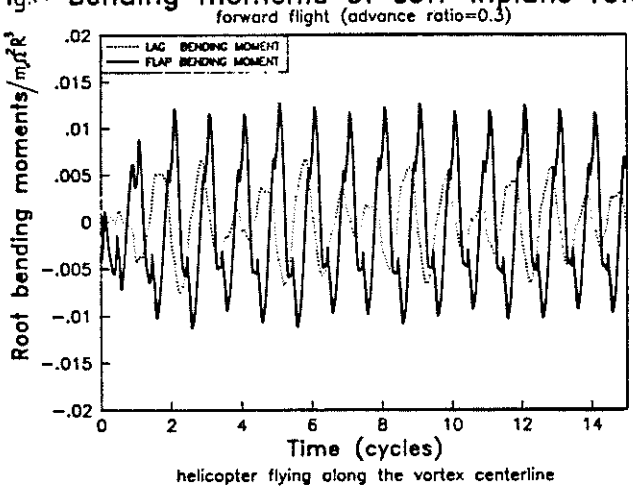

Fig.15 Hub moments of soft-inplane rotor

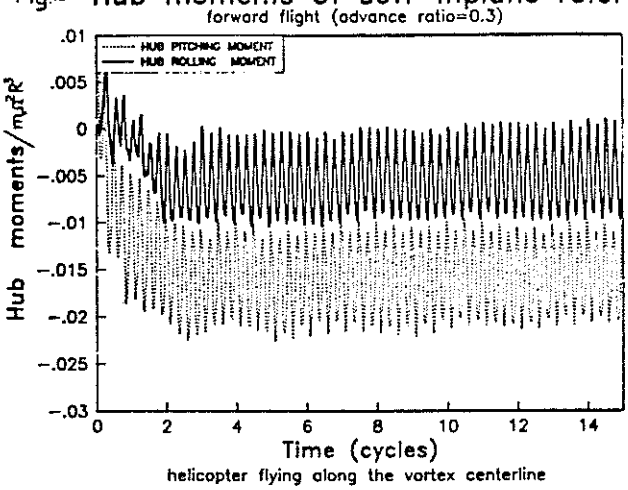

Fig16 Dynamic response of soft-inplane rotor

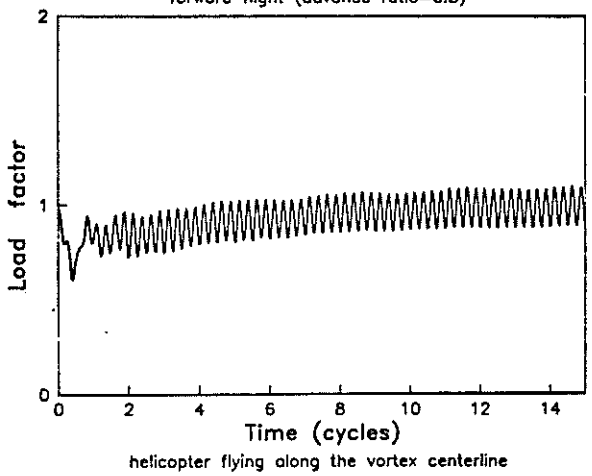

Fig.17 Flap, lag torsion bending deflections

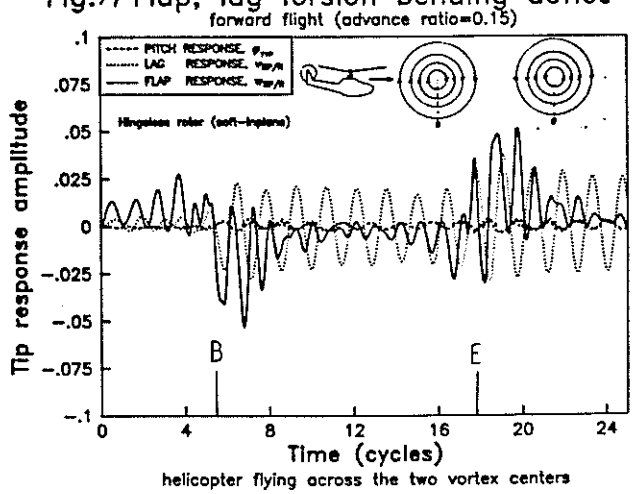

Fig.18 Disk tilt variation with time

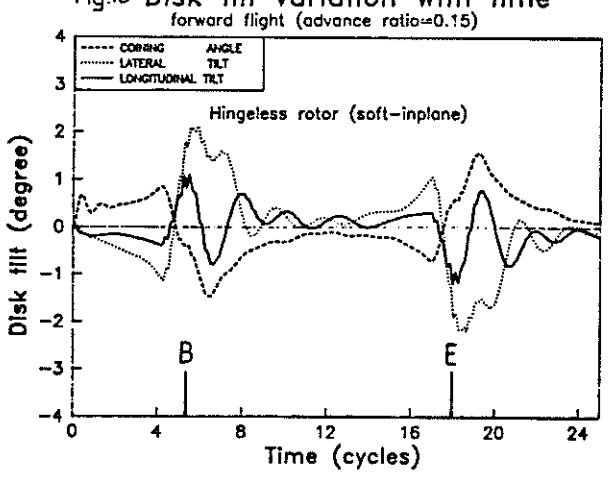

Fig.19 Blade bending moments

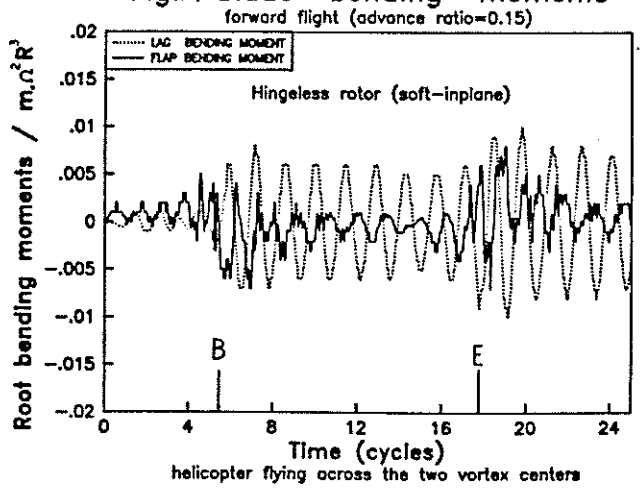

Fig.20 Hub moments of soft-inplane rotor

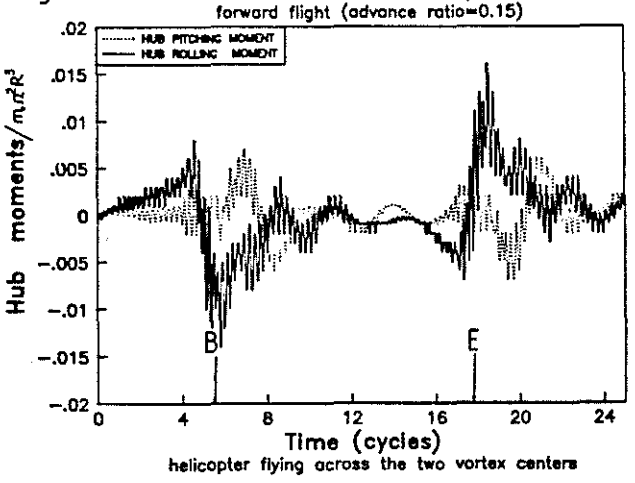

Fig.21 Dynamic response of soft-inplane rotor

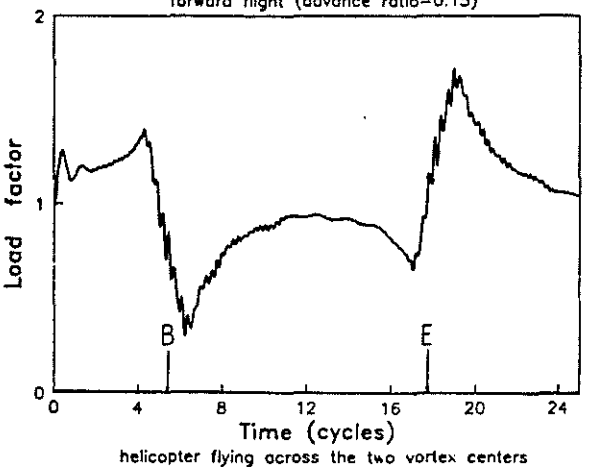

Fig.22 Flap, lag torsion bending deflections

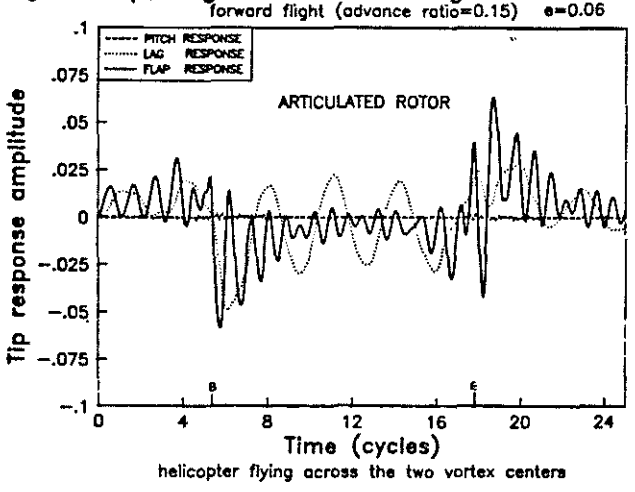

Fig.23 Disk tilt variation with time

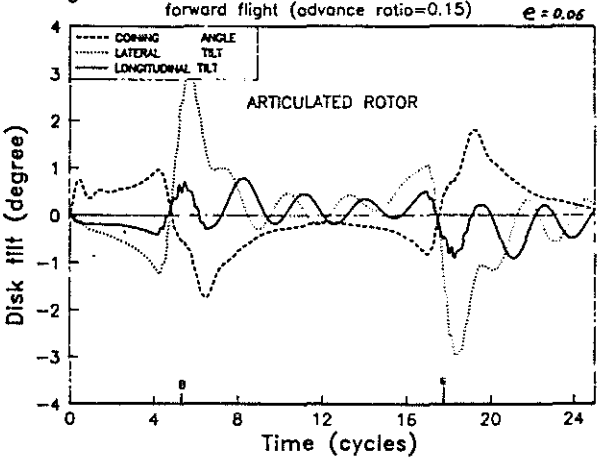

Fig.24 Hub moments of articulated rotor

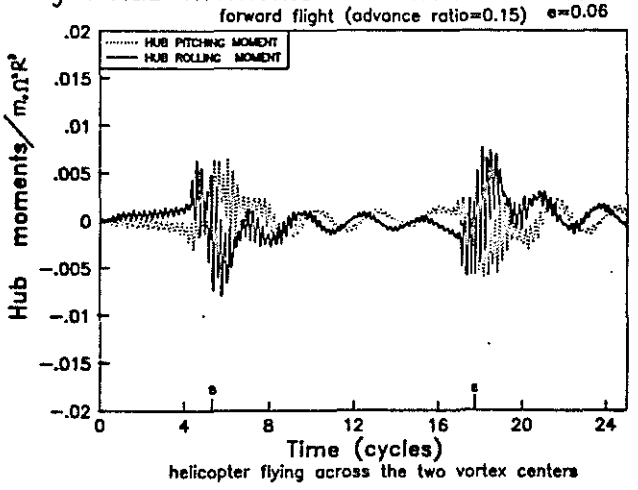

Fig.25 Dynamic response of articulated rotor

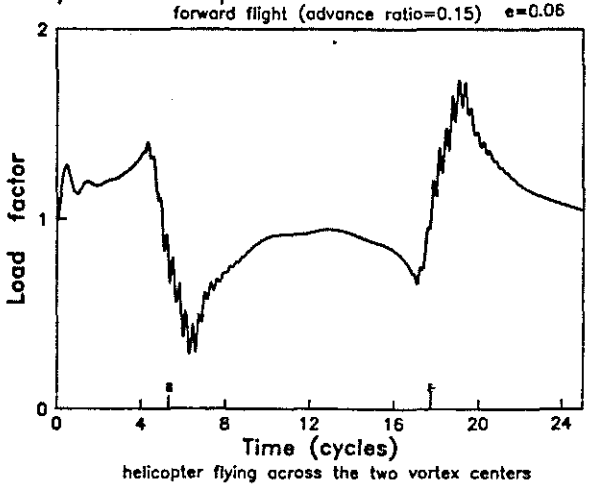

Fig.26 Flap, lag torsion bending deflections

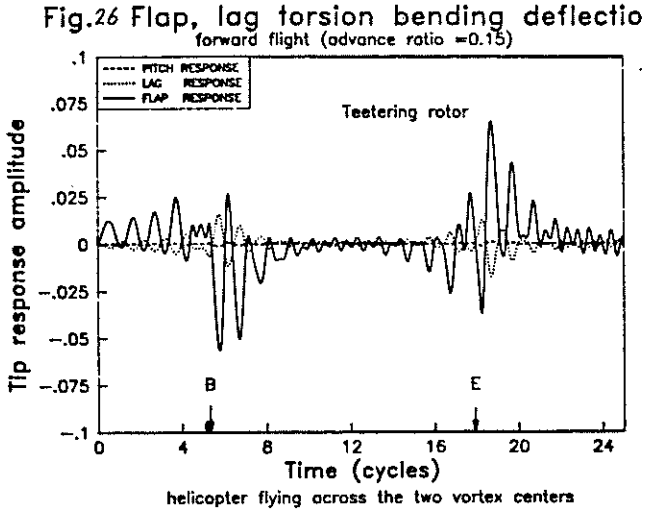

Fig.27 Bending moments of teetering rotor

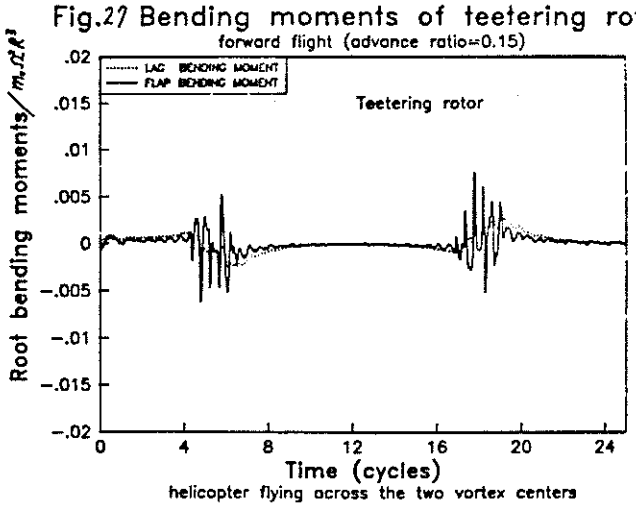

Fig.28 Hub moments of teetering rotor

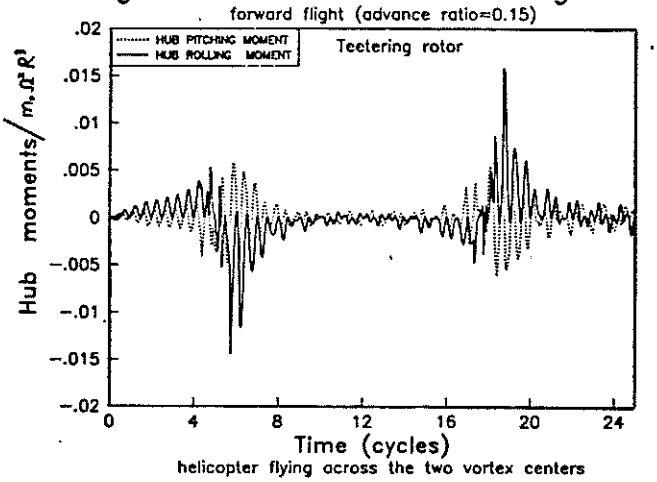

Fig.29 Dynamic response of teetering rotor